Integrated Force/Motion Trajectory Design of Parallel Robots for Singularity Robustness during Contact Tasks

Mustafa Özdemir[1,*] and Sıtkı Kemal İder[2]

[1] Department of Mechanical Engineering, Faculty of Engineering, Marmara University, Recep Tayyip Erdoğan Campus, 34854 Maltepe, İstanbul, Türkiye
E-mail: mustafa.ozdemir@marmara.edu.tr
ORCID iD: https://orcid.org/0000-0002-4981-9573
* Corresponding author

[2] Department of Mechanical Engineering, Faculty of Engineering, Çankaya University, 06790 Etimesgut, Ankara, Türkiye
E-mail: kider@cankaya.edu.tr
ORCID iD: https://orcid.org/0000-0001-5869-893X

Abstract: Parallel robots have an increasing use in industrial and medical applications. Many of these applications require the execution of contact tasks. However, parallel robots possess drive singularities, which act as invisible barriers inside their workspace. In this paper, we develop an integrated force and motion trajectory planning method for removing drive singularities of parallel robots which perform contact tasks. The method is based on satisfaction of a consistency condition at the singularity, which is stated in terms of the generalized velocities, accelerations and contact forces, provided that the derivative of the associated determinant with respect to time does not simultaneously vanish. It is shown that, in the presence of singularity crossing, either the motion or the force trajectory can be arbitrarily chosen while the other is planned to satisfy the necessary conditions.

Keywords: parallel robot; contact task; motion trajectory; force trajectory; drive singularity; singularity removal

1 Introduction

In order to increase profitability and market share, firms seek ways to improve efficiency and competitiveness in their manufacturing processes. The use of robotics emerges as one of the most effective tools for achieving these goals [1, 2], especially at an accelerated pace in the era of Industry 4.0 [3-6]. Another area where the utilization of robots is of vital importance is medicine [7, 8]. Robotic-

assisted systems enable to perform high-precision surgical operations with minimal invasion [9, 10].

Conventional robotic arms have a serial kinematic architecture. However, parallel robots offer better accuracy and precision, increased rigidity, larger load capacity, lower inertias, and higher accelerations and speeds compared to the serial ones [11-14]. Owing to these advantages they have received attention as motion simulators [11, 15]. In addition, they have been widely applied to various industrial purposes, including, but not limited to, pick-and-place tasks [16], welding applications [17], spray-painting [18], and machining operations [12, 19]. They have been also increasingly used as medical and surgical robots [20].

One of the most serious handicaps of parallel robots is the limitation in the usability of their workspace due to the "type II singularity" loci within it [21]. The actuator forces tend to infinity in magnitude near singularities of this type. Due to this fact, they are alternatively called "drive singularities" [22, 23].

Since their avoidance during path planning would confine the robot to only a small portion of the workspace, there has been a growing interest in developing different methods for dealing with drive singularities. The approaches in this regard fall into two main categories. The first of these is to use actuation redundancy, which is well known in the literature to decrease or eliminate singularities [24]. The second one focuses on nonredundant parallel robots with an aim to obtain bounded inverse dynamics solutions near singularities.

This relatively new second approach enables parallel robots to pass in a controllable fashion through drive singular configurations and hence to use their entire workspace at no extra cost. The motion trajectory must be planned to sustain the consistency of the equations of motion at the singular configuration to be passed through [23, 25, 26]. The necessary "consistency conditions" were derived by Ider [23], and Briot and Arakelian [26] with different physical interpretations. As another recent effort in this regard, Ozgoren [27] obtained a similar condition by using the virtual work method.

However, as shown by Özdemir [28-30] there exist also "high-order" or "hyper-" drive singularities where boundedness of the inverse dynamics solution cannot be guaranteed only via the said consistency considerations. Özdemir [28] proved that time derivatives of the vanishing determinant should also be taken into account for removal of drive singularities. In accordance with this desingularization principle, Özdemir and İder [31] developed a motion trajectory planning method for flexible-joint parallel robots.

Although there are a number of unconstrained motion tasks such as pick-and-place and spray-painting operations [32-34], numerous advanced applications require the end-effector to move along a prescribed trajectory on a constraint surface while exerting a specified contact force profile onto that constraint surface. Some typical examples of these constrained motion tasks are machining processes (e.g.,

cutting, grinding, deburring), assembly operations and surgical procedures [32-37]. Indeed, it is essential to control the contact forces for executing such interaction tasks. Thus, in the last decade there has been a considerable research focus on force/position control of parallel robots [38-43].

However, in the previous studies on parallel robots performing contact tasks, singularity crossing problem is not considered. In order to fill this gap in the literature, the aim of the present paper is to develop an integrated force and motion trajectory planning method for enabling parallel robots to perform contact tasks in the presence of drive singularities. A condition is formulated for ensuring the consistency of the motion and force trajectories at the singularity. In accordance with the literature [28-30], the occurrence of high-order singularities is also prevented. Hence, boundedness of the actuator torques and forces near the singularity time of the contact task is guaranteed. We believe that the current study will facilitate the prevalence of parallel robots in industrial and medical applications.

2 Mathematical Modelling of a Parallel Robot Performing a Contact Task

Consider an n degree-of-freedom rigid-link rigid-joint parallel robot with n actuators. For modelling purposes, let this robot be transformed into an $m > n$ degree-of-freedom tree-like open system by cutting some passive joints. We denote the vector of the tree-like system's joint variables by $\boldsymbol{\theta} = \begin{bmatrix} \theta_1 & \theta_2 & \cdots & \theta_m \end{bmatrix}^{\mathrm{T}}$. By reconnecting the cut joints, the loop-closure equations can be written as

$$f_i(\boldsymbol{\theta}) = 0, \quad i = 1, 2, \ldots, m-n \tag{1}$$

Differentiating equations (1) with respect to time t and rearranging into matrix form, we get

$$\mathbf{A}\dot{\boldsymbol{\theta}} = \mathbf{0} \tag{2}$$

where the elements of the $(m-n)\times m$ matrix $\mathbf{A} = \mathbf{A}(\boldsymbol{\theta})$ are given by

$$A_{ij} = \frac{\partial f_i}{\partial \theta_j}, \quad i = 1, 2, \ldots, m-n, \quad j = 1, 2, \ldots, m \tag{3}$$

Assuming that the environment is stationary and rigid, the constraints due to the contact of the end-effector with the environment can be expressed as

$$g_u(\boldsymbol{\theta}) = 0, \quad u = 1, 2, \ldots, k \tag{4}$$

where k is the number of contact constraints such that $k < n$. These contact constraints can be written at velocity level as

$$\mathbf{B}\dot{\boldsymbol{\theta}} = \mathbf{0} \tag{5}$$

where the elements of the $k \times m$ matrix $\mathbf{B} = \mathbf{B}(\boldsymbol{\theta})$ are

$$B_{uj} = \frac{\partial g_u}{\partial \theta_j}, \quad u = 1, 2, \ldots, k, \quad j = 1, 2, \ldots, m \tag{6}$$

It is worth mentioning that the contact constraints considered here are equality constraints. This is because the robot is assumed not to lose its contact with the constraint surface during the whole task [44].

Selecting $\boldsymbol{\theta}$ as the vector of generalized coordinates, neglecting the impact and friction effects, and using the Lagrangian method, the equations of constrained motion of the parallel robot can be obtained in the following form:

$$\mathbf{M}\ddot{\boldsymbol{\theta}} + \mathbf{N} = \mathbf{T} + \mathbf{A}^{\mathrm{T}}\boldsymbol{\lambda} + \mathbf{B}^{\mathrm{T}}\boldsymbol{\mu} \tag{7}$$

where $\mathbf{M} = \mathbf{M}(\boldsymbol{\theta})$ is the $m \times m$ generalized mass matrix, $\mathbf{N} = \mathbf{N}(\boldsymbol{\theta}, \dot{\boldsymbol{\theta}})$ the m-dimensional vector of generalized Coriolis, centrifugal and gravity forces, and $\mathbf{T}$ the m-dimensional vector of nonconservative generalized forces applied by the actuators. In these equations, $\boldsymbol{\lambda} = \begin{bmatrix} \lambda_1 & \lambda_2 & \cdots & \lambda_{m-n} \end{bmatrix}^{\mathrm{T}}$ is the vector of the Lagrange multipliers associated with the loop-closure constraints, whereas $\boldsymbol{\mu} = \begin{bmatrix} \mu_1 & \mu_2 & \cdots & \mu_k \end{bmatrix}^{\mathrm{T}}$ is the vector of the Lagrange multipliers due to the contact constraints.

Let $\mathbf{x} = \begin{bmatrix} x_1 & x_2 & \cdots & x_n \end{bmatrix}^{\mathrm{T}}$ be the vector of independent motion variables of the end-effector when it is in free motion. However, only $n-k$ of them can be arbitrarily prescribed along the contact surface. In other words, the number of motion degrees of freedom reduces to $n-k$. Denote by $\mathbf{y} = \begin{bmatrix} y_1 & y_2 & \cdots & y_{n-k} \end{bmatrix}^{\mathrm{T}}$ the vector of independent variables of contact motion, which are related to the joint variables by

$$y_v = h_v(\boldsymbol{\theta}), \quad v = 1, 2, \ldots, n-k \tag{8}$$

By taking the time derivative of equations (8) and putting into matrix form, we obtain

$$\dot{\mathbf{y}} = \mathbf{C}\dot{\boldsymbol{\theta}} \tag{9}$$

where the elements of the $(n-k) \times m$ matrix $\mathbf{C} = \mathbf{C}(\boldsymbol{\theta})$ are given by

$$C_{vj} = \frac{\partial h_v}{\partial \theta_j}, \quad v = 1, 2, \ldots, n-k, \quad j = 1, 2, \ldots, m \tag{10}$$

3 Conditions for Singularity Robust Driving During a Contact Task

The vector $\boldsymbol{\theta}$ can be assumed to be constructed such that its first n elements are the actuated joint variables. Notice that this assumption yields no loss of generality since it deals only with ordering of the vector elements. Under this assumption, the vector $\mathbf{T}$ is of the form

$$\mathbf{T} = \begin{bmatrix} \boldsymbol{\tau} \\ \mathbf{0} \end{bmatrix} \tag{11}$$

where τ_w denotes the generalized actuator force that is associated with the generalized coordinate θ_w ($w = 1, 2, \ldots, n$) and $\boldsymbol{\tau} = \begin{bmatrix} \tau_1 & \tau_2 & \tau_n \end{bmatrix}^{\mathrm{T}}$. The above form of $\mathbf{T}$ suggests the following partitioning of the matrices $\mathbf{M}$, $\mathbf{A}$, $\mathbf{B}$ and the vector $\mathbf{N}$:

$$\mathbf{M} = \begin{bmatrix} \mathbf{M}^{\mathrm{a}}_{n\times m} \\ \mathbf{M}^{\mathrm{u}}_{(m-n)\times m} \end{bmatrix} \tag{12}$$

$$\mathbf{A} = \begin{bmatrix} \mathbf{A}^{\mathrm{a}}_{(m-n)\times n} & \mathbf{A}^{\mathrm{u}}_{(m-n)\times(m-n)} \end{bmatrix} \tag{13}$$

$$\mathbf{B} = \begin{bmatrix} \mathbf{B}^{\mathrm{a}}_{k\times n} & \mathbf{B}^{\mathrm{u}}_{k\times(m-n)} \end{bmatrix} \tag{14}$$

$$\mathbf{N} = \begin{bmatrix} \mathbf{N}^{\mathrm{a}}_{n\times 1} \\ \mathbf{N}^{\mathrm{u}}_{(m-n)\times 1} \end{bmatrix} \tag{15}$$

where the sizes of the submatrices and subvectors are shown as subscripts. Then, using equations (11)-(15), one can rewrite equation (7) in the following form:

$$\boldsymbol{\tau} = \mathbf{M}^{\mathrm{a}}\ddot{\boldsymbol{\theta}} + \mathbf{N}^{\mathrm{a}} - \left(\mathbf{A}^{\mathrm{a}}\right)^{\mathrm{T}}\boldsymbol{\lambda} - \left(\mathbf{B}^{\mathrm{a}}\right)^{\mathrm{T}}\boldsymbol{\mu} \tag{16}$$

$$\left(\mathbf{A}^{\mathrm{u}}\right)^{\mathrm{T}}\boldsymbol{\lambda} = \mathbf{M}^{\mathrm{u}}\ddot{\boldsymbol{\theta}} + \mathbf{N}^{\mathrm{u}} - \left(\mathbf{B}^{\mathrm{u}}\right)^{\mathrm{T}}\boldsymbol{\mu} \tag{17}$$

In order to determine the joint motions required for a given motion trajectory $\mathbf{y}(t)$ along the constraint surface, equations (2), (5) and (9) can be merged into the following equation:

$$\mathbf{D}\dot{\boldsymbol{\theta}} = \mathbf{z} \tag{18}$$

where $\mathbf{D} = \mathbf{D}(\boldsymbol{\theta})$ is an $m \times m$ matrix constructed as

$$\mathbf{D} = \begin{bmatrix} \mathbf{A} \\ \mathbf{B} \\ \mathbf{C} \end{bmatrix} \tag{19}$$

and $\mathbf{z} = \mathbf{z}(t)$ is an m-dimensional vector defined as

$$\mathbf{z} = \begin{bmatrix} \mathbf{0} \\ \dot{\mathbf{y}} \end{bmatrix} \tag{20}$$

As long as $\mathbf{D}$ is nonsingular, equation (18) constitutes a system of m first-order differential equations that can be rewritten as

$$\dot{\boldsymbol{\theta}} = \mathbf{D}^{-1}\mathbf{z} \tag{21}$$

By time-differentiating equation (18) and rearranging, one can also get

$$\ddot{\boldsymbol{\theta}} = \mathbf{D}^{-1}\left(-\dot{\mathbf{D}}\dot{\boldsymbol{\theta}} + \dot{\mathbf{z}}\right) \tag{22}$$

Thus, once the system of equation (21) is solved for the generalized coordinates $\boldsymbol{\theta}(t)$ and the generalized velocities $\dot{\boldsymbol{\theta}}(t)$ by a suitable numerical integration method, the generalized accelerations $\ddot{\boldsymbol{\theta}}(t)$ can be computed from equation (22).

Substituting the calculated $\boldsymbol{\theta}$, $\dot{\boldsymbol{\theta}}$ and $\ddot{\boldsymbol{\theta}}$ together with the given force trajectory $\boldsymbol{\mu}(t)$ into equation (17) and solving for $\boldsymbol{\lambda}(t)$ gives the following equation, provided that $\mathbf{A}^{\mathrm{u}}$ is nonsingular:

$$\boldsymbol{\lambda} = \left(\mathbf{A}^{\mathrm{u}}\right)^{-\mathrm{T}}\left[\mathbf{M}^{\mathrm{u}}\ddot{\boldsymbol{\theta}} + \mathbf{N}^{\mathrm{u}} - \left(\mathbf{B}^{\mathrm{u}}\right)^{\mathrm{T}}\boldsymbol{\mu}\right] \tag{23}$$

Finally, the required actuator forces can be computed from equation (16).

During the implementation of the above procedure, inverse kinematic singularities occur when the determinant of the $\mathbf{D}$ matrix becomes zero. However, such singularities are in general on the boundaries of the workspace [21]. Therefore, they are not a major concern and are left out of the scope of this study.

Drive singularities arise when the determinant of the $\mathbf{A}^{\mathrm{u}}$ matrix vanishes. As it is apparent from equation (23), the Lagrange multipliers associated with the loop-closure constraints grow without bounds in the neighborhood of such singularities. Let us assume that $\mathbf{A}^{\mathrm{u}}$ is rank deficient by one at the drive singular configuration to be passed through. This assumption is quite realistic since higher rank deficiencies would be rather rare in practice [23, 25]. By writing $\left(\mathbf{A}^{\mathrm{u}}\right)^{-\mathrm{T}}$ in terms of the adjoint matrix and determinant of $\left(\mathbf{A}^{\mathrm{u}}\right)^{\mathrm{T}}$, equation (23) can be reexpressed as

$$\boldsymbol{\lambda} = \frac{1}{\det\left(\left(\mathbf{A}^{\mathrm{u}}\right)^{\mathrm{T}}\right)} \operatorname{adj}\left(\left(\mathbf{A}^{\mathrm{u}}\right)^{\mathrm{T}}\right)\left[\mathbf{M}^{\mathrm{u}}\ddot{\boldsymbol{\theta}} + \mathbf{N}^{\mathrm{u}} - \left(\mathbf{B}^{\mathrm{u}}\right)^{\mathrm{T}}\boldsymbol{\mu}\right] \tag{24}$$

or, recalling that $\det\left(\left(\mathbf{A}^{\mathrm{u}}\right)^{\mathrm{T}}\right) = \det\left(\mathbf{A}^{\mathrm{u}}\right)$ and $\operatorname{adj}\left(\left(\mathbf{A}^{\mathrm{u}}\right)^{\mathrm{T}}\right) = \left(\operatorname{adj}\left(\mathbf{A}^{\mathrm{u}}\right)\right)^{\mathrm{T}}$,

$$\boldsymbol{\lambda} = \frac{1}{\det\left(\mathbf{A}^{\mathrm{u}}\right)}\left(\operatorname{adj}\left(\mathbf{A}^{\mathrm{u}}\right)\right)^{\mathrm{T}}\left[\mathbf{M}^{\mathrm{u}}\ddot{\boldsymbol{\theta}} + \mathbf{N}^{\mathrm{u}} - \left(\mathbf{B}^{\mathrm{u}}\right)^{\mathrm{T}}\boldsymbol{\mu}\right] \tag{25}$$

By inspecting equation (25), the condition that should be satisfied for the dynamic equations of the robot to be consistent at a drive singularity can be stated as

$$\left(\operatorname{adj}\left(\mathbf{A}^{\mathrm{u}}\right)\right)^{\mathrm{T}}\left[\mathbf{M}^{\mathrm{u}}\ddot{\boldsymbol{\theta}} + \mathbf{N}^{\mathrm{u}} - \left(\mathbf{B}^{\mathrm{u}}\right)^{\mathrm{T}}\boldsymbol{\mu}\right] = \mathbf{0} \tag{26}$$

If this consistency condition holds and the first-order time derivative of the determinant $\det\left(\mathbf{A}^{\mathrm{u}}\right)$ does not vanish at the singularity time t_{s} (i.e., the singularity is not of high order), then it follows from l'Hôpital's Rule that $\lim_{t\to t_{\mathrm{s}}} \lambda_i(t)$ is finite for all $i = 1, 2, \ldots, m-n$, which further implies that the required actuator forces will remain bounded as the singularity is approached. However, the inverse dynamics solution is still indeterminate at time t_{s} since satisfaction of the condition given by equation (26) for maintaining the consistency of the robot's dynamic equations yields $0/0$ in equation (25) for all $\lambda_i(t_{\mathrm{s}})$. This indeterminacy can be removed by setting

$$\lambda_i(t_{\mathrm{s}}) = \lim_{t\to t_{\mathrm{s}}} \lambda_i(t), \quad i = 1, 2, \ldots, m-n \tag{27}$$

where the limits $\lim_{t\to t_{\mathrm{s}}} \lambda_i(t)$ are evaluated via l'Hôpital's Rule.

If the consistency condition given by equation (26) is not satisfied, then at least one of the limits $\lim_{t\to t_{\mathrm{s}}} \lambda_i(t)$ is not finite, which yields an unbounded growth of the inverse dynamics solution in the vicinity of the singularity. Besides, it is useful to note that among the $m-n$ individual equations of the matrix equation (26), only one is linearly independent. This is due to the fact [45] that the adjoint matrix of a matrix that is rank deficient by one has rank one.

4 Case Study

In this section, the application of the developed method is exemplified by considering the planar 5R parallel robot, which is shown in Figure 1. Link 0 is the fixed link. Each moving link p ($p = 1, 2, 3, 4$) has mass m_p, mass center at G_p, and centroidal moment of inertia I_{G_p}. The link lengths are denoted by $L_0 = |R_1R_2|$, $L_1 = |R_1R_3|$, $L_2 = |R_2R_4|$, $L_3 = |R_3R_5|$ and $L_4 = |R_4R_5|$. The locations of the mass centers are given by $r_1 = |R_1G_1|$, $\alpha_1 = \angle R_3R_1G_1$, $r_2 = |R_2G_2|$, $\alpha_2 = \angle R_4R_2G_2$, $r_3 = |R_3G_3|$, $\alpha_3 = \angle R_5R_3G_3$, $r_4 = |R_4G_4|$ and $\alpha_4 = \angle R_5R_4G_4$. The origin of the fixed rectangular coordinate system xy is at joint R_1. The gravitational acceleration g acts in the negative y-direction. The robot has two degrees of freedom and is actuated by two motors that are located at joints R_1 and R_2. The endpoint P is given by $b = |R_3P|$ and $\beta = \angle R_5R_3P$.

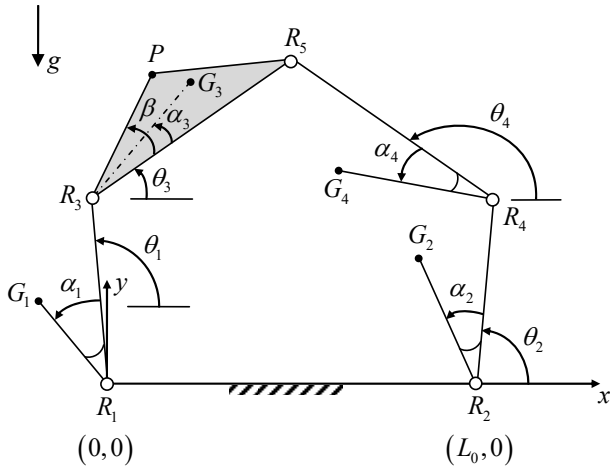

Figure 1
The considered robot

By virtually cutting the closed-loop at joint R_5 and choosing the generalized coordinates vector as $\boldsymbol{\theta} = [\theta_1 \quad \theta_2 \quad \theta_3 \quad \theta_4]^{\mathrm{T}}$, the generalized mass matrix and the vector of generalized nonlinear inertial and gravity forces of the resulting open-loop system can be obtained as

$$\mathbf{M} = \begin{bmatrix} M_{11} & 0 & M_{13} & 0 \\ 0 & M_{22} & 0 & M_{24} \\ M_{31} & 0 & M_{33} & 0 \\ 0 & M_{42} & 0 & M_{44} \end{bmatrix} \tag{28}$$

$$\mathbf{N} = \begin{bmatrix} N_1 \\ N_2 \\ N_3 \\ N_4 \end{bmatrix} \tag{29}$$

where

$$M_{11} = m_1 r_1^2 + I_{G_1} + m_3 L_1^2 \tag{30}$$

$$M_{13} = M_{31} = m_3 r_3 L_1 \cos\left(\theta_1 - \theta_3 - \alpha_3\right) \tag{31}$$

$$M_{22} = m_2 r_2^2 + I_{G_2} + m_4 L_2^2 \tag{32}$$

$$M_{24} = M_{42} = m_4 r_4 L_2 \cos\left(\theta_2 - \theta_4 - \alpha_4\right) \tag{33}$$

$$M_{33} = m_3 r_3^2 + I_{G_3} \tag{34}$$

$$M_{44} = m_4 r_4^2 + I_{G_4} \tag{35}$$

$$N_1 = m_3 r_3 L_1 \dot{\theta}_3^2 \sin\left(\theta_1 - \theta_3 - \alpha_3\right) + m_1 g r_1 \cos\left(\theta_1 + \alpha_1\right) + m_3 g L_1 \cos\theta_1 \tag{36}$$

$$N_2 = m_4 r_4 L_2 \dot{\theta}_4^2 \sin\left(\theta_2 - \theta_4 - \alpha_4\right) + m_2 g r_2 \cos\left(\theta_2 + \alpha_2\right) + m_4 g L_2 \cos\theta_2 \tag{37}$$

$$N_3 = -m_3 r_3 L_1 \dot{\theta}_1^2 \sin\left(\theta_1 - \theta_3 - \alpha_3\right) + m_3 g r_3 \cos\left(\theta_3 + \alpha_3\right) \tag{38}$$

$$N_4 = -m_4 r_4 L_2 \dot{\theta}_2^2 \sin\left(\theta_2 - \theta_4 - \alpha_4\right) + m_4 g r_4 \cos\left(\theta_4 + \alpha_4\right) \tag{39}$$

Then, by reconnecting joint R_5, the loop-closure equations can be written as

$$f_1(\boldsymbol{\theta}) = L_1 \cos\theta_1 + L_3 \cos\theta_3 - L_0 - L_2 \cos\theta_2 - L_4 \cos\theta_4 = 0 \tag{40}$$

$$f_2(\boldsymbol{\theta}) = L_1 \sin\theta_1 + L_3 \sin\theta_3 - L_2 \sin\theta_2 - L_4 \sin\theta_4 = 0 \tag{41}$$

Thus, the Jacobian matrix of the loop-closure constraint equations is

$$\mathbf{A} = \begin{bmatrix} -L_1 \sin\theta_1 & L_2 \sin\theta_2 & -L_3 \sin\theta_3 & L_4 \sin\theta_4 \\ L_1 \cos\theta_1 & -L_2 \cos\theta_2 & L_3 \cos\theta_3 & -L_4 \cos\theta_4 \end{bmatrix} \tag{42}$$

As illustrated in Figure 2, let the constrained-motion task of the robot be moving the endpoint P according to a prescribed trajectory $x_P(t)$ on the frictionless plane surface given by $y = y^*$ while simultaneously applying a specified normal contact force $\mu(t)$ onto it. The surface is rigid and fixed in space. The robot will be in contact with the surface only at point P throughout the entire duration, t_f, of the task.

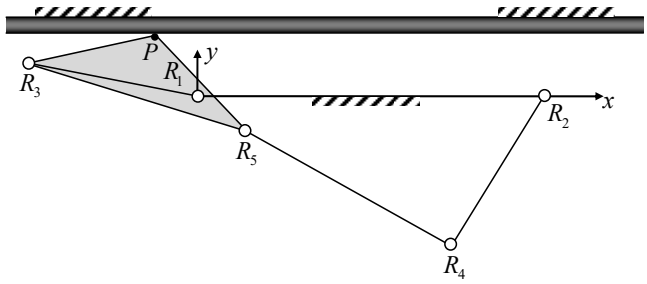

Figure 2
The given contact task

The motion trajectory can be expressed as

$$x_P(t) = x_0 + (x_f - x_0)\, s(t) \tag{43}$$

where x_0 and x_f are the initial and final values of the x-coordinate of point P on the constraint surface, and $s(t)$ is a timing function, which is chosen to be the following quintic polynomial in order to have zero initial and final velocities and accelerations:

$$s(t) = 6\left(\frac{t}{t_f}\right)^5 - 15\left(\frac{t}{t_f}\right)^4 + 10\left(\frac{t}{t_f}\right)^3 \tag{44}$$

Let the force trajectory $\mu(t)$ be trapezoidal. The desired constant value of the contact force in the plateau phase is μ^*. The force will be linearly increased from zero to this value in the first Δt time units of motion and will be decreased linearly back to zero in the last Δt time units. Thus,

$$\mu(t) = \begin{cases} \dfrac{t}{\Delta t}\mu^*, & 0 \le t < \Delta t \\ \mu^*, & \Delta t \le t < t_f - \Delta t \\ \dfrac{t_f - t}{\Delta t}\mu^*, & t_f - \Delta t \le t \le t_f \end{cases} \tag{45}$$

The surface contact constraint can be expressed in the task space as

$$g_1(x_P, y_P) = y^* - y_P = 0 \tag{46}$$

or in the joint space as

$$g_1(\boldsymbol{\theta}) = y^* - L_1 \sin\theta_1 - b\sin(\theta_3 + \beta) = 0 \tag{47}$$

Thus, the vector of generalized constraint forces acting on the robot due to its contact with the surface at point P is

$$\mathbf{F}_{\mathrm{c}} = \mathbf{B}^{\mathrm{T}} \mu \tag{48}$$

where

$$\mathbf{B} = \begin{bmatrix} -L_1 \cos\theta_1 & 0 & -b\cos\left(\theta_3 + \beta\right) & 0 \end{bmatrix} \tag{49}$$

The motion variable x_P can be related to the joint variables as

$$x_P = h_1\left(\boldsymbol{\theta}\right) = L_1 \cos\theta_1 + b\cos\left(\theta_3 + \beta\right) \tag{50}$$

Then, it follows from equations (10) that

$$\mathbf{C} = \begin{bmatrix} -L_1 \sin\theta_1 & 0 & -b\sin\left(\theta_3 + \beta\right) & 0 \end{bmatrix} \tag{51}$$

After constructing the matrix $\mathbf{D}$ given by equation (19), the condition for the occurrence of an inverse kinematic singularity can be expressed as follows:

$$\det\left(\mathbf{D}\right) = L_1 L_2 L_4 b \sin\left(\theta_1 - \theta_3 - \beta\right)\sin\left(\theta_4 - \theta_2\right) = 0 \tag{52}$$

With $n = 2$, $m = 4$ and $k = 1$, the $\mathbf{M}$, $\mathbf{A}$ and $\mathbf{B}$ matrices and the $\mathbf{N}$ vector are partitioned according to equations (12)-(15) as given below:

$$\mathbf{M}^{\mathrm{a}} = \begin{bmatrix} M_{11} & 0 & M_{13} & 0 \\ 0 & M_{22} & 0 & M_{24} \end{bmatrix} \tag{53}$$

$$\mathbf{M}^{\mathrm{u}} = \begin{bmatrix} M_{31} & 0 & M_{33} & 0 \\ 0 & M_{42} & 0 & M_{44} \end{bmatrix} \tag{54}$$

$$\mathbf{A}^{\mathrm{a}} = \begin{bmatrix} -L_1 \sin\theta_1 & L_2 \sin\theta_2 \\ L_1 \cos\theta_1 & -L_2 \cos\theta_2 \end{bmatrix} \tag{55}$$

$$\mathbf{A}^{\mathrm{u}} = \begin{bmatrix} -L_3 \sin\theta_3 & L_4 \sin\theta_4 \\ L_3 \cos\theta_3 & -L_4 \cos\theta_4 \end{bmatrix} \tag{56}$$

$$\mathbf{B}^{\mathrm{a}} = \begin{bmatrix} -L_1 \cos\theta_1 & 0 \end{bmatrix} \tag{57}$$

$$\mathbf{B}^{\mathrm{u}} = \begin{bmatrix} -b\cos\left(\theta_3 + \beta\right) & 0 \end{bmatrix} \tag{58}$$

$$\mathbf{N}^{\mathrm{a}} = \begin{bmatrix} N_1 \\ N_2 \end{bmatrix} \tag{59}$$

$$\mathbf{N}^{\mathrm{u}} = \begin{bmatrix} N_3 \\ N_4 \end{bmatrix} \tag{60}$$

Then the equation describing the drive singularity locus in the joint space can be obtained as

$$\det\left(\mathbf{A}^{\mathrm{u}}\right) = L_3 L_4 \sin\left(\theta_3 - \theta_4\right) = 0 \tag{61}$$

Readers can be referred to numerous studies [29, 46-48] for more details on the singularities and workspace of the planar 5R mechanism.

The values of the model parameters are chosen as follows: $L_0 = 3$ m, $L_1 = L_2 = 1.5$ m, $L_3 = L_4 = 2$ m, $b = 1$ m, $\beta = \left(\pi/6\right)$ rad, $m_1 = m_2 = 0.4$ kg, $m_3 = m_4 = 0.6$ kg, $r_1 = r_2 = 0.75$ m, $r_3 = 1.5$ m, $r_4 = 1$ m, $\alpha_1 = \alpha_2 = 0$, $\alpha_3 = \alpha_4 = \left(2\pi/3\right)$ rad, $I_{G_1} = I_{G_2} = 0.2$ kg·m^2, $I_{G_3} = I_{G_4} = 0.3$ kg·m^2. The gravitational acceleration is assumed to be $g = 9.807$ m/s^2. The constraint surface is taken as $y^* = 0.5$ m. The x-coordinates of the starting and ending positions of the endpoint P along this surface are $x_0 = -0.5$ m and $x_{\mathrm{f}} = -0.42$ m, respectively. The total duration of the task is selected to be $t_{\mathrm{f}} = 2$ s. Thus, the timing function becomes

$$s\left(t\right) = 0.1875t^5 - 0.9375t^4 + 1.25t^3 \tag{62}$$

The motion trajectory obtained using equation (43) is shown in Figure 3. The values of the joint variables at the starting position of the endpoint are as follows: $\theta_1 = 169.4°$, $\theta_2 = 237.5°$, $\theta_3 = 343.0°$, $\theta_4 = 151.5°$. In the case studies presented below, the numerical integrations are based on the Dormand-Prince formula (see, e.g., [49] and the references cited therein) with a fixed step size of 0.002 s.

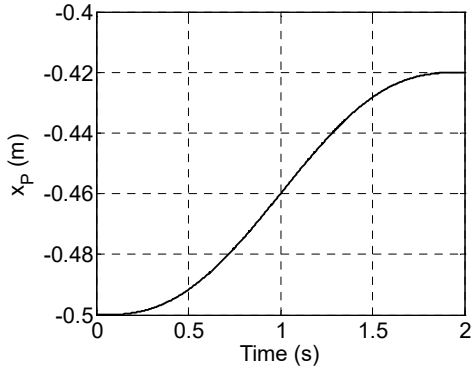

Figure 3
The desired motion trajectory

4.1 Case 1: A Case Where Motion and Force Trajectories Are Not Consistent with Each Other at the Singularity

As the first case, let the force trajectory be generated with $\mu^* = 1\,\text{N}$ and $\Delta t = 0.2\,\text{s}$, as shown in Figure 4.

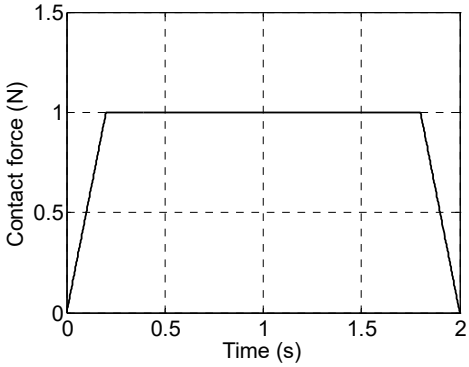

Figure 4
A force trajectory that is not consistent with the motion trajectory at the singularity

The inverse kinematic solution is singularity free. The time variations of the joint angular displacements that correspond to the prescribed motion trajectory of the endpoint on the constraint surface are shown in Figure 5.

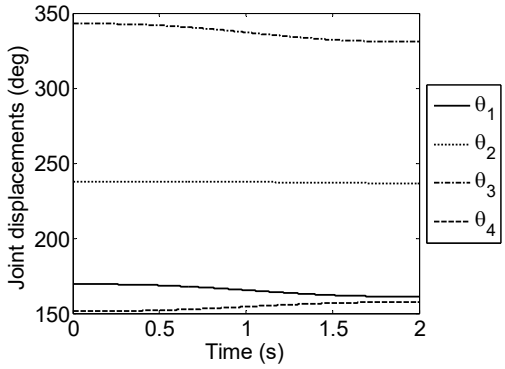

Figure 5
Time histories of the joint variables necessary for the desired constrained motion of the end-effector

However, although no inverse kinematic singularity is encountered, a drive singularity occurs when $x_P = -0.45\,\text{m}$ (i.e., $s = 0.65$). The values of the joint variables at this singular position are as follows: $\theta_1 = 164.2°$, $\theta_2 = 237.4°$, $\theta_3 = 335.3°$, $\theta_4 = 155.3°$. Both Lagrange multipliers become unbounded near this position. As can be read from Figure 6, the singularity time is $t_s = 1.164\,\text{s}$.

The limits of the required motor torques as t approaches this value are not finite, as can be seen in Figure 7.

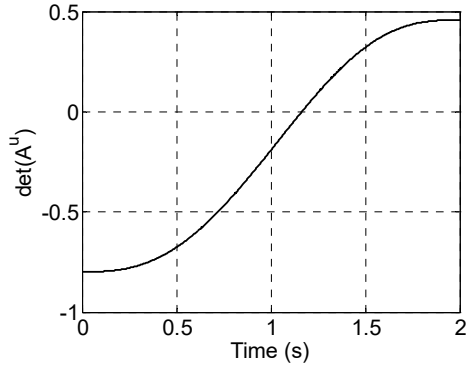

Figure 6
Time variation of the determinant whose vanishing implies the occurrence of a drive singularity

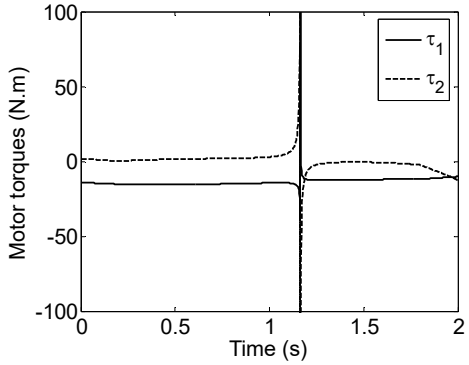

Figure 7
Motor torques required for the motion and force trajectories that are not consistent with each other at the singularity

4.2 Case 2: A Case Where Motion and Force Trajectories Are Consistent with Each Other at the Singularity

In order to overcome the unboundedness of the inverse dynamics solution, the motion and force trajectories should be such that the consistency of the dynamic equations is maintained at the singular configuration to be passed through. The consistency condition that should be satisfied at the singular position of interest can be derived as follows: The transpose of the adjoint matrix of $\mathbf{A}^{\mathrm{u}}$ is

$$\left(\mathrm{adj}\left(\mathbf{A}^{\mathrm{u}}\right)\right)^{\mathrm{T}} = \begin{bmatrix} -L_4\cos\theta_4 & -L_3\cos\theta_3 \\ -L_4\sin\theta_4 & -L_3\sin\theta_3 \end{bmatrix} \tag{63}$$

Substituting equation (63) into equation (26) gives

$$\begin{aligned} &-L_4 \cos\theta_4 \left[M_{31}\ddot{\theta}_1 + M_{33}\ddot{\theta}_3 + N_3 + \mu b \cos\left(\theta_3 + \beta\right) \right] \\ &-L_3 \cos\theta_3 \left(M_{42}\ddot{\theta}_2 + M_{44}\ddot{\theta}_4 + N_4 \right) = 0 \end{aligned} \tag{64}$$

$$\begin{aligned} &-L_4 \sin\theta_4 \left[M_{31}\ddot{\theta}_1 + M_{33}\ddot{\theta}_3 + N_3 + \mu b \cos\left(\theta_3 + \beta\right) \right] \\ &-L_3 \sin\theta_3 \left(M_{42}\ddot{\theta}_2 + M_{44}\ddot{\theta}_4 + N_4 \right) = 0 \end{aligned} \tag{65}$$

The following relation in radians exists between θ_3 and θ_4 at the encountered singular configuration: $\theta_4 = \theta_3 - \pi$. Thus, at that singularity, $\cos\theta_4 = -\cos\theta_3$, $\sin\theta_4 = -\sin\theta_3$, the rank of $\left(\text{adj}\left(\mathbf{A}^{\text{u}}\right)\right)^{\text{T}}$ is one, and equations (64) and (65) are linearly dependent and can be reduced to

$$L_4 \left[M_{31}\ddot{\theta}_1 + M_{33}\ddot{\theta}_3 + N_3 + \mu b \cos\left(\theta_3 + \beta\right) \right] - L_3 \left(M_{42}\ddot{\theta}_2 + M_{44}\ddot{\theta}_4 + N_4 \right) = 0 \tag{66}$$

The above consistency condition can be satisfied at the singularity via a proper planning of either the motion or the force trajectory. The velocity- and acceleration-level inverse kinematic solutions are calculated at the encountered singularity as

$$\dot{\theta}_1\left(t_{\text{s}}\right) = -1.8461\dot{x}_P\left(t_{\text{s}}\right) \tag{67}$$

$$\dot{\theta}_2\left(t_{\text{s}}\right) = -0.2892\dot{x}_P\left(t_{\text{s}}\right) \tag{68}$$

$$\dot{\theta}_3\left(t_{\text{s}}\right) = -2.6766\dot{x}_P\left(t_{\text{s}}\right) \tag{69}$$

$$\dot{\theta}_4\left(t_{\text{s}}\right) = 1.3388\dot{x}_P\left(t_{\text{s}}\right) \tag{70}$$

$$\ddot{\theta}_1\left(t_{\text{s}}\right) = -4.4386\left[\dot{x}_P\left(t_{\text{s}}\right)\right]^2 - 1.8461\ddot{x}_P\left(t_{\text{s}}\right) \tag{71}$$

$$\ddot{\theta}_2\left(t_{\text{s}}\right) = -9.3659\left[\dot{x}_P\left(t_{\text{s}}\right)\right]^2 - 0.2892\ddot{x}_P\left(t_{\text{s}}\right) \tag{72}$$

$$\ddot{\theta}_3\left(t_{\text{s}}\right) = -4.3744\left[\dot{x}_P\left(t_{\text{s}}\right)\right]^2 - 2.6766\ddot{x}_P\left(t_{\text{s}}\right) \tag{73}$$

$$\ddot{\theta}_4\left(t_{\text{s}}\right) = 1.7241\left[\dot{x}_P\left(t_{\text{s}}\right)\right]^2 + 1.3388\ddot{x}_P\left(t_{\text{s}}\right) \tag{74}$$

In the above equations, the endpoint velocity is in m/s, endpoint acceleration is in m/s^2, angular joint velocities are in rad/s, and angular joint accelerations are in rad/s^2. Then, for the singular configuration of interest, we compute from equations (31) and (33)-(35) that $M_{31}\left(t_{\text{s}}\right) = 0.4854\ \text{kg}\cdot\text{m}^2$, $M_{33} = 1.65\ \text{kg}\cdot\text{m}^2$,

$M_{42}(t_s) = 0.7096\ \text{kg}\cdot\text{m}^2$, $M_{44} = 0.9\ \text{kg}\cdot\text{m}^2$, and from equations (38) and (39) that

$$N_3(t_s) = -4.2931\left[\dot{x}_P(t_s)\right]^2 - 0.8179 \tag{75}$$

$$N_4(t_s) = 0.0463\left[\dot{x}_P(t_s)\right]^2 + 0.5452 \tag{76}$$

where N_3 and N_4 are obtained in N·m for the endpoint velocity in m/s. By substituting these into equation (66), simplifying and multiplying both sides of the resulting equation by -1, we get

$$12.6244\ddot{x}_P(t_s) + 17.2351\left[\dot{x}_P(t_s)\right]^2 - 1.9914\mu(t_s) + 2.7262 = 0 \tag{77}$$

Equation (77) shows that consistent values of the endpoint velocity, the endpoint acceleration and the contact force at the singularity time lie on a quadric surface as seen in Figure 8. In this figure, v_P and a_P represent the endpoint velocity and acceleration, respectively. It may be useful to note that $v_P = \dot{x}_P$ and $a_P = \ddot{x}_P$ since the endpoint moves along a constant y path.

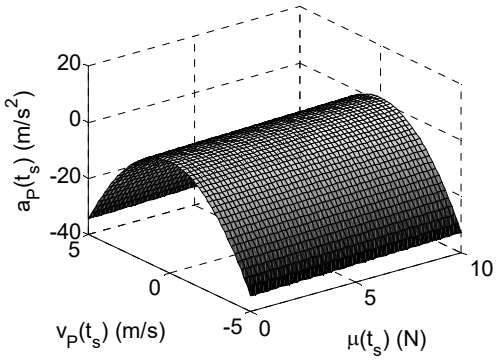

Figure 8
Consistent values of the endpoint velocity, the endpoint acceleration and the contact force at the singular point of interest

In this example, we prefer to plan the force trajectory for satisfying the consistency condition. Hence, the previously chosen desired motion trajectory becomes realizable, despite the presence of drive singularity. We first compute that $\dot{x}_P(t_s) = 0.0710$ m/s and $\ddot{x}_P(t_s) = -0.0478\ \text{m/s}^2$. Then, substituting these values into equation (77), we get $\mu(t_s) = 1.11$ N. As our second case, we construct a new trapezoidal force trajectory with $\mu^* = 1.11$ N and $\Delta t = 0.2$ s, as shown in Figure 9. With this new force trajectory, the dynamic equations are now

consistent at all times. Additionally, $\det\left(\mathbf{A}^{\mathrm{u}}\right)$ has a nonzero first-order time derivative at the singularity time. Thus, the required motor torques remain bounded in the neighborhood of the singularity, as can be seen in Figure 10. It is useful to note that $\lim_{t\to t_s}\lambda_1(t) = 4.77$ N and $\lim_{t\to t_s}\lambda_2(t) = -1.93$ N.

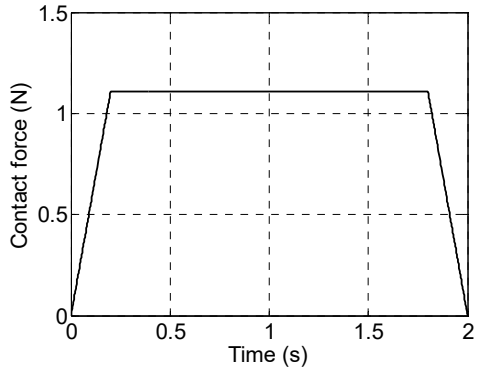

Figure 9
A force trajectory that is consistent with the motion trajectory at the singularity

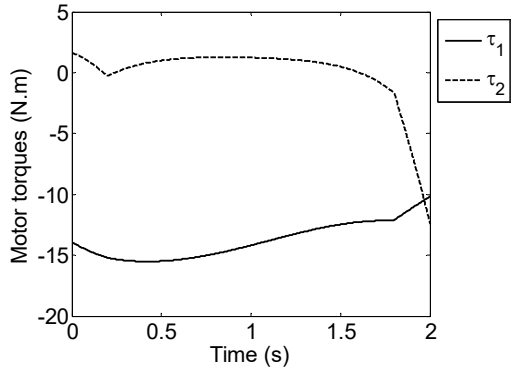

Figure 10
Motor torques required for the motion and force trajectories that are consistent with each other at the singularity

Conclusions

This paper presents an integrated force and motion trajectory planning approach for removing drive singularities of parallel robots performing contact tasks. Such tasks constitute the majority of the industrial and medical robotic applications. A consistency condition is derived in terms of the generalized velocities, accelerations and contact forces. This condition should be considered while planning the motion and force trajectories. Also, in accordance with the literature

[28-30], the singularity is prevented from being of high order. Thus, the boundedness of the inverse dynamics solution around the singularity is ensured.

The effectiveness of the proposed method is verified through a numerical case study where the planar 5R parallel robot is considered to perform a constrained motion task in the presence of drive singularities. It is shown that one of the motion and force trajectories can be arbitrarily chosen while the other is planned to satisfy the consistency condition at the singularity. The consistent values of the endpoint velocity, the endpoint acceleration and the contact force at the singularity are found to describe a quadric surface.

References

[1] M. Smieszek, P. Dobrzanski and M. Dobrzanska. Comparison of the level of robotisation in Poland and selected countries, including social and economic factors. *Acta Polytechnica Hungarica*, 16(4):197-212, 2019

[2] Z. Cséfalvay. Robotization in Central and Eastern Europe: catching up or dependence? *European Planning Studies*, 28(8):1534-1553, 2020

[3] G. Haidegger and I. Paniti. Episodes of robotics and manufacturing automation achievements from the past decades and vision for the next decade. *Acta Polytechnica Hungarica*, 16(10):119-136, 2019

[4] A. Okanović, B. Jokanović, V. Đaković, S. Vukadinović and J. Ješić. Innovating a model for measuring competitiveness in accordance with the challenges of Industry 4.0. *Acta Polytechnica Hungarica*, 17(7):67-88, 2020

[5] W. S. Barbosa, M. M. Gioia, V. G. Natividade, R. F. F. Wanderley, M. R. Chaves, F. C. Gouvea and F. M. Gonçalves. Industry 4.0: examples of the use of the robotic arm for digital manufacturing processes. *International Journal on Interactive Design and Manufacturing (IJIDeM)*, 14(4):1569-1575, 2020

[6] G. Fragapane, D. Ivanov, M. Peron, F. Sgarbossa and J. O. Strandhagen. Increasing flexibility and productivity in Industry 4.0 production networks with autonomous mobile robots and smart intralogistics. *Annals of Operations Research*, 308(1-2):125-143, 2022

[7] Á. Takács, D. Á. Nagy, I. J. Rudas and T. Haidegger. Origins of surgical robotics: From space to the operating room. *Acta Polytechnica Hungarica*, 13(1):13-30, 2016

[8] P. E. Dupont, B. J. Nelson, M. Goldfarb, B. Hannaford, A. Menciassi, M. K. O'Malley, N. Simaan, P. Valdastri and G.-Z. Yang. A decade retrospective of medical robotics research from 2010 to 2020. *Science Robotics*, 6(60):eabi8017, 2021

[9] M. J. Mack. Minimally invasive and robotic surgery. *JAMA-Journal of the American Medical Association*. 285(5):568-572, 2001

[10] R. Nagyné Elek and T. Haidegger. Robot-assisted minimally invasive surgical skill assessment—manual and automated platforms. *Acta Polytechnica Hungarica*, 16(8):141-169, 2019

[11] J.-P. Merlet. Parallel Robots, 2nd edition. In: Solid Mechanics and Its Applications, Volume 128, Series Editor: G. M. L. Gladwell, Springer, Dordrecht, 2006

[12] Y. Jin, H. Chanal and F. Paccot. Parallel Robots. In: Handbook of Manufacturing Engineering and Technology, A. Y. C. Nee (Ed.), Springer, London, 2015, pp. 2091-2127

[13] J. Somló, G. D. Varga, M. Zenkl and B. Mikó. The „Phantom" Delta robot A new device for parallel robot investigations. *Acta Polytechnica Hungarica*, 15(4):143-160, 2018

[14] J. Somló. General triangle parallel robot (GTPR) Basic features of a new robot type - kinematics and related application issues. *Acta Polytechnica Hungarica*, 16(5):7-24, 2019

[15] G. Liu, Z. Qu, J. Han and X. Liu. Systematic optimal design procedures for the Gough-Stewart platform used as motion simulators. *Industrial Robot*, 40(6):550-558, 2013

[16] F. Bourbonnais, P. Bigras and I. A. Bonev. Minimum-time trajectory planning and control of a pick-and-place five-bar parallel robot. *IEEE/ASME Transactions on Mechatronics*, 20(2):740-749, 2015

[17] J. Shi, Y. Wang, G. Zhang and H. Ding. Optimal design of 3-DOF PKM module for friction stir welding. *The International Journal of Advanced Manufacturing Technology*, 66(9-12):1879-1889, 2013

[18] J. Wu, Y. Gao, B. Zhang and L. Wang. Workspace and dynamic performance evaluation of the parallel manipulators in a spray-painting equipment. *Robotics and Computer-Integrated Manufacturing*, 44:199-207, 2017

[19] J. Jahanpour, M. Motallebi and M. Porghoveh. A novel trajectory planning scheme for parallel machining robots enhanced with NURBS curves. *Journal of Intelligent & Robotic Systems*, 82(2):257-275, 2016

[20] H. Tian, C. Wang, X. Dang and L. Sun. A 6-DOF parallel bone-grinding robot for cervical disc replacement surgery. *Medical & Biological Engineering & Computing*, 55(12):2107-2121, 2017

[21] C. Gosselin and J. Angeles. Singularity analysis of closed-loop kinematic chains. *IEEE Transactions on Robotics and Automation*, 6(3):281-290, 1990

[22] S. K. Ider. Singularity robust inverse dynamics of planar 2-RPR parallel manipulators. *Proceedings of the Institution of Mechanical Engineers, Part C: Journal of Mechanical Engineering Science*, 218(7):721-730, 2004

[23] S. K. Ider. Inverse dynamics of parallel manipulators in the presence of drive singularities. *Mechanism and Machine Theory*, 40(1):33-44, 2005

[24] M. Luces, J. K. Mills and B. Benhabib. A review of redundant parallel kinematic mechanisms. *Journal of Intelligent & Robotic Systems*, 86(2):175-198, 2017

[25] C. K. K. Jui and Q. Sun. Path tracking of parallel manipulators in the presence of force singularity. *ASME Journal of Dynamic Systems, Measurement, and Control*, 127(4):550-563, 2005

[26] S. Briot and V. Arakelian. Optimal force generation in parallel manipulators for passing through the singular positions. *The International Journal of Robotics Research*, 27(8):967-983, 2008

[27] M. K. Ozgoren. Kinematic and kinetostatic analysis of parallel manipulators with emphasis on position, motion, and actuation singularities. *Robotica*, 37(4):599-625, 2019

[28] M. Özdemir. Removal of singularities in the inverse dynamics of parallel robots. *Mechanism and Machine Theory*, 107:71-86, 2017

[29] M. Özdemir. High-order singularities of 5R planar parallel robots. *Robotica*, 37(2):233-245, 2019

[30] M. Özdemir. Hypersingularities of 3-RRR planar parallel robots. *Proceedings of the Romanian Academy, Series A: Mathematics, Physics, Technical Sciences, Information Science*, 22(4):353-360, 2021

[31] M. Özdemir and S. K. İder. Desingularization of flexible-joint parallel robots. *Acta Polytechnica Hungarica*, 18(6):85-106, 2021

[32] G. de A. Barreto, A. F. R. Araújo and H. J. Ritter. Self-organizing feature maps for modeling and control of robotic manipulators. *Journal of Intelligent & Robotic Systems*, 36(4):407-450, 2003

[33] M. Vukobratovic, V. Potkonjak and V. Matijevic. Dynamics of Robots with Contact Tasks. In: International Series on Microprocessor-Based and Intelligent Systems Engineering, Volume 26, Series Editor: S. G. Tzafestas, Springer, Dordrecht, 2003

[34] M. Vukobratovic. Robot-environment dynamic interaction survey and future trends. *Journal of Computer and Systems Sciences International*, 49(2):329-342, 2010

[35] E. Dombre, G. Duchemin, P. Poignet and F. Pierrot. Dermarob: A safe robot for reconstructive surgery. *IEEE Transactions on Robotics and Automation*, 19(5):876-884, 2003

[36] N. Zemiti, G. Morel, T. Ortmaier and N. Bonnet. Mechatronic design of a new robot for force control in minimally invasive surgery. *IEEE/ASME Transactions on Mechatronics*, 12(2):143-153, 2007

[37] A. Pappalardo, A. Albakri, C. Liu, L. Bascetta, E. De Momi and P. Poignet. Hunt–Crossley model based force control for minimally invasive robotic surgery. *Biomedical Signal Processing and Control*, 29:31-43, 2016

[38] S. Bellakehal, N. Andreff, Y. Mezouar and M. Tadjine. Force/position control of parallel robots using exteroceptive pose measurements. *Meccanica*, 46(1):195-205, 2011

[39] M. Madani and M. Moallem. Hybrid position/force control of a flexible parallel manipulator. *Journal of the Franklin Institute*, 348(6):999-1012, 2011

[40] B. Achili, B. Daachi, Y. Amirat, A. Ali-Cherif and M. E. Daâchi. A stable adaptive force/position controller for a C5 parallel robot: a neural network approach. *Robotica*, 30(7):1177-1187, 2012

[41] O. Korkmaz and S. K. Ider. Hybrid force and motion control of flexible joint parallel manipulators using inverse dynamics approach. *Advanced Robotics*, 28(18):1221-1230, 2014

[42] J. Cazalilla, M. Vallés, Á. Valera, V. Mata and M. Díaz-Rodríguez. Hybrid force/position control for a 3-DOF 1T2R parallel robot: Implementation, simulations and experiments. *Mechanics Based Design of Structures and Machines*, 44(1-2):16-31, 2016

[43] C. Gao, D. Cong, X. Liu, Z. Yang and H. Tao. Hybrid position/force control of 6-dof hydraulic parallel manipulator using force and vision. *Industrial Robot*, 43(3):274-283, 2016

[44] L. Villani and J. De Schutter. Force Control. In: Springer Handbook of Robotics, B. Siciliano and O. Khatib (Eds.), Springer, Berlin, Heidelberg, 2008, pp. 161-185

[45] M. J. Tobias. Matrices in Engineering Problems. In: Synthesis Lectures on Mathematics and Statistics, Series Editor: S. G. Krantz, Morgan & Claypool Publishers, 2011

[46] G. Alıcı. Determination of singularity contours for five-bar planar parallel manipulators. *Robotica*, 18(5):569-575, 2000

[47] J. J. Cervantes-Sánchez, J. C. Hernández-Rodríguez and J. G. Rendón-Sánchez. On the workspace, assembly configurations and singularity curves of the RRRRR-type planar manipulator. *Mechanism and Machine Theory*, 35(8):1117-1139, 2000

[48] E. Macho, O. Altuzarra, C. Pinto and A. Hernandez. Workspaces associated to assembly modes of the 5R planar parallel manipulator. *Robotica*, 26(3):395-403, 2008

[49] A. D. Polyanin and V. F. Zaitsev. Handbook of Ordinary Differential Equations: Exact Solutions, Methods, and Problems. Chapman & Hall/CRC Press, Taylor & Francis Group, Boca Raton, Florida, USA, 2018